Journal of Alloys and Compounds 480 (2009) 917–921

Contents lists available at ScienceDirect

Journal of Alloys and Compounds

journal homepage: www.elsevier.com/locate/jallcom

Pressure-induced phase transition in AlN: An *ab initio* molecular dynamics study

Murat Durandurdu [a,b,*]

[a] *Department of Physics, University of Texas at El Paso, El Paso, TX 79968, USA*
[b] *Fizik Bölümü, Ahi Evran Üniversitesi, Kırşehir 40100, Turkey*

ARTICLE INFO

Article history:
Received 8 January 2009
Received in revised form 14 February 2009
Accepted 18 February 2009
Available online 4 March 2009

Keywords:
Semiconductor
Phase transformation
Molecular dynamics

ABSTRACT

An *ab initio* constant pressure technique is applied to study the pressure-induced phase transition in AlN. A first-order phase transformation from the wurtzite structure to a rocksalt structure is observed in the constant pressure simulations. The transformation proceeds via two fivefold coordinated intermediate states within $P6_3/mmc$ and *Cmcm* symmetry. The influence of pressure on the electronic structure of AlN is also investigated. The computed pressure coefficients and deformation potential are in good agreement with the earlier first principles calculations.

1. Introduction

Aluminum nitride (AlN) has attracted much attention in recent years because of its great potential for high-technology applications. It is an electronic ceramic and has remarkable physical properties [1–4] such as a high melting point, a high thermal conductivity, good dielectric strength and high hardness. Also AlN has a direct energy band gap of 6.2 eV [5]. These properties make AlN an ideal material for microelectronic substrate applications, shortwavelength light-emitting diodes, laser diodes, and optical detectors, as well as for high-temperature, high-power, and high-frequency devices.

At ambient pressure, AlN crystallizes in a hexagonal wurtzite (WZ) structure with space group $P6_3mc$ and has a very small lattice constant $a = 3.108$ Å and $c/a = 1.60113$ comparing the value of $c/a = 1.633$ for an ideal WZ structure [6]. AlN has four atoms per unit cell in the WZ structure. It has a mixture of covalent bonding and ionic tetrahedral bonding. AlN can also crystallize in the zinc blende (ZB) cubic structure with the space group $F\bar{4}3m$. The ZB state of AlN is stable only when it is very thin 1.5–2.0 nm and it converts to the WZ structure at larger thickness [7].

AlN transforms from the WZ structure-to-the rocksalt (RS) structure ($Fm\bar{3}m$) with the application of pressure [6,8,9]. This phase transition displays a rather large hysteresis, with persistence of the RS state [6]. This behavior makes it very difficult to locate the coexistence pressure for the two phases. The stability of both phases of AlN has been also investigated using the first principles calculations and the WZ-to-RS phase transition is predicted to occur about 8.3–16.0 GPa [10–16], in agreement with the experimental transition pressures of 14.0–22.0 GPa [6,8,9]. However, a clear atomic level picture of this phase transition, specifically the transformation mechanism of the WZ-to-RS phase transition of AlN, could not be addressed in these studies.

For the WZ-to-RS phase transformation, the hexagonal and tetragonal mechanisms have been proposed. In the hexagonal path, a WZ structure is first compressed along the *c*-axis, resulting into a fivefold coordinated hexagonal intermediate state with space group $P6_3/mmc$ and then a RS phase form through the opening of the hexagonal angle. In the tetragonal pathway, the two-step process found in the hexagonal pathway is reversed. Saitta and Decremps [13] analyzed both tetragonal and hexagonal intermediate states for some WZ-structured bulk materials through *ab initio* calculations of the full phonon properties and suggested that the transformation pathway of the WZ crystals depends on the presence of *d* electrons on cation atoms. In particular, they proposed that the hexagonal transformation path is only possible for the semiconductors containing light (*d* electron free) cations such as SiC and AlN while the tetragonal phase is favorable in materials whose cations have *d* electrons such as GaN, CdS, ZnO. The energy landscape calculations also suggest that AlN likely follows the hexagonal path [16].

The conclusions of Ref. [13] were however challenged by recent experimental and theoretical studies [17,18]. Furthermore, recent simulations proposed multiple transformation mechanisms with almost the same energy barrier for CdSe [19]. To our knowledge, the direct observation of the transition pathway of AlN has not been observed in any constant pressure simulation and hence the transformation mechanism of AlN still remains an open question.

* Correspondence address: Department of Physics, University of Texas at El Paso, 500 W. University Ave, El Paso, TX 79968, USA.
E-mail address: mdurandurdu@utep.edu.

0925-8388/$ – see front matter © 2009 Elsevier B.V. All rights reserved.
doi:10.1016/j.jallcom.2009.02.060

In this study, we carry out constant pressure *ab initio* simulations to fully explain the microscopic nature of the pressure-induced phase transition of AlN and to compare its behavior with the other WZ type materials [19–23]. Our findings demonstrate that the WZ-to-RS phase change follows the hexagonal pathway and involve two fivefold coordinated intermediates states with the space group of $P6_3/mmc$ and *Cmcm*. Additionally, we study the influence of the applied pressure on the electronic properties of AlN and find that the band gap energy gradually increases with increasing pressure. Our computed pressure coefficients and deformation potential are in good agreement with the previous first principle calculations.

2. Computational method

We used the first-principles pseudopotentials method within the density-functional theory (DFT) and the generalized gradient approximation of Perdew et al. for the exchange–correlation energy [24]. The calculation was carried out with the *ab initio* program SIESTA [25] using a linear combination of atomic orbitals as the basis set, and norm-conservative Troullier–Martins pseudopotential [26]. The pseudopotential cut-off radii for Al was 2.28 bohr for the *s* and *p* channels and 1.24 bohr for the N *s* and *p* channels. A split-valence single-ξ basis set was employed. A uniform mesh with a plane wave cut-off of 150 Ry was used to represent the electron density, the local part of the pseudopotentials, and the Hartree and the exchange–correlation potential. The simulation cell consists of 72 atoms with periodic boundary conditions. We used Γ-point sampling for the Brillouin zone integration. The molecular dynamics (MD) simulations were performed using the NPH (constant number of atoms, constant pressure, and constant enthalpy) ensemble. The reason for choosing this ensemble is to remove the thermal fluctuation, which facilitates easier examination of the structure during the phase transformation. Pressure was applied via the method of Parrinello and Rahman [27] and the structure is equilibrated with a period of 1000 time steps (each time step is 2.5 femto-second (fs)) at each applied pressure. We also used the power quenching technique during the MD simulations. In this technique, each velocity component is quenched individually. At each time step, if the force and velocity components have opposite sign, the velocity component is set equal to zero. All atoms or supercell velocities (for cell shape optimizations) are then allowed to accelerate at the next time step.

In order to determine the intermediate state during the phase transformation, we used the KPLOT program [28] that supplies detailed information about space group, cell parameters and atomic position of a given structure. For the symmetry analysis we used 0.2 Å, 4°, and 0.7 Å tolerances for bond lengths, bond angles and interplanar spacing, respectively.

3. Results

We first relax our 72 atoms supercell at zero pressure to calculate the lattice parameters of the WZ phase and then compare them with available experimental and theoretical data. The equilibrium unit cell lattice constants of AlN are found to be $a = 3.139$ Å, and $c/a = 1.614$ Å. These values are comparable with the experimental results of $a = 3.108$ Å and $c/a = 1.601$ Å [29,30] and the previous theoretical results of $a = 3.06$–3.151 Å and $c/a = 1.57$–1.612 Å [12,30–33]. The internal parameter *u*, proportional to the Al–N bond length along the *c*-axis, is determined to be 0.38, which is again comparable with the experimental and theoretical values of 0.38–0.383 [30–33]. These results suggest that the parameters used in the simulations are good enough to study the pressure-induced phase transition of AlN using the constant pressure *ab initio* technique.

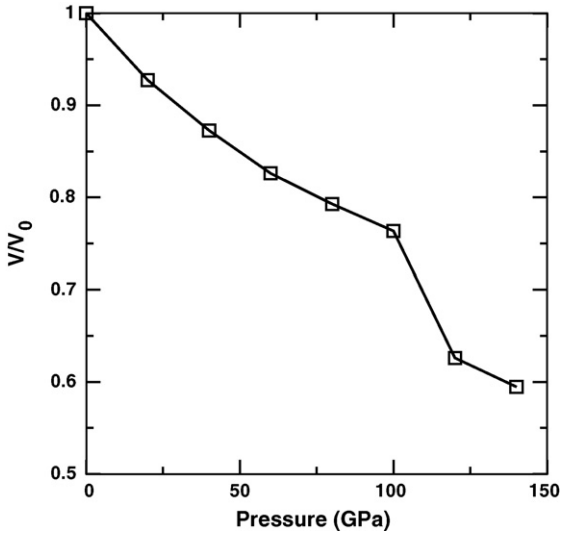

Fig. 1. Volume change of AlN as a function of pressure. When the applied pressure is increased from 100 GPa to 120 GPa, the volume dramatically decreases, implying a first-order phase transformation. At 120 GPa, the wurtzite structure transforms a rocksalt structure in the constant pressure *ab initio* simulations.

The pressure–volume relation obtained through the constant pressure *ab initio* simulation is given in Fig. 1. The volume presents a sharp change when the applied pressure is increased from 100 GPa to 120 GPa, indicating a first-order pressure-induced phase transition in AlN. The structural analysis reveals that the WZ structure transforms into a RS phase at this pressure as shown in Fig. 2. This finding shows that the *ab initio* technique successfully generates the experiment observed high-pressure phase of AlN with an overestimated transition pressure, relative to the experimental transition pressure of 14–22.0 GPa [6,8,9]. Such an overestimation in transition pressures, in analogous to superheating MD simulations, is usually seen in constant pressure simulations and implies a high intrinsic activation barrier for transforming one solid phase into another in simulations. When the particular conditions such as finite size of the simulation cell, the lack of any defect in simulated structure, the time scale of simulations, etc. are considered, such an overestimated transition pressure is anticipated [34]. On the other hand, the thermodynamic theorem does not take into account the possible existence of such an activation barrier separating the two structural phases. Therefore, as a next step, we consider the energy–volume calculations to study the stability of the WZ and RS phases. We fit their energy–volume data to the third-order Birch–Murnaghan equation of state. Since at the phase transition, the two phases have the same enthalpy ($H = E_{tot} + PV$, where $P = -\mathrm{d}E_{tot}/\mathrm{d}V$ is obtained by direct differentiation of the calculated the energy–volume curves), the transition pressure can be easily determined by equating the enthalpy of the two phases. The computed enthalpy curve of the WZ and RS states as a function of pressure is shown in Fig. 3. We obtain a transition pressure of about 17.8 GPa, which is comparable with the experimental result of 14–22 GPa [6,8,9] and the values of 8.3–16 GPa predicted in the previous DFT calculations [10–16].

From the energy–volume relation we also calculate the bulk properties of the WZ and RS states. The bulk modulus (B_o) and its pressure derivative (B'_o) of the WZ are estimated as 198 GPa and 6.2, respectively. These values are in good agreement with experimental and theoretical results of 184–233 GPa and 3.55–6.3 [6,10–16,30–33]. For the RS state, B_o and B'_o are calculated to be 253 GPa and 4.19, respectively, which are also comparable with the experimental and theoretical results of 215–295 GPa and 3.5–4.8 [10–16,30,33].

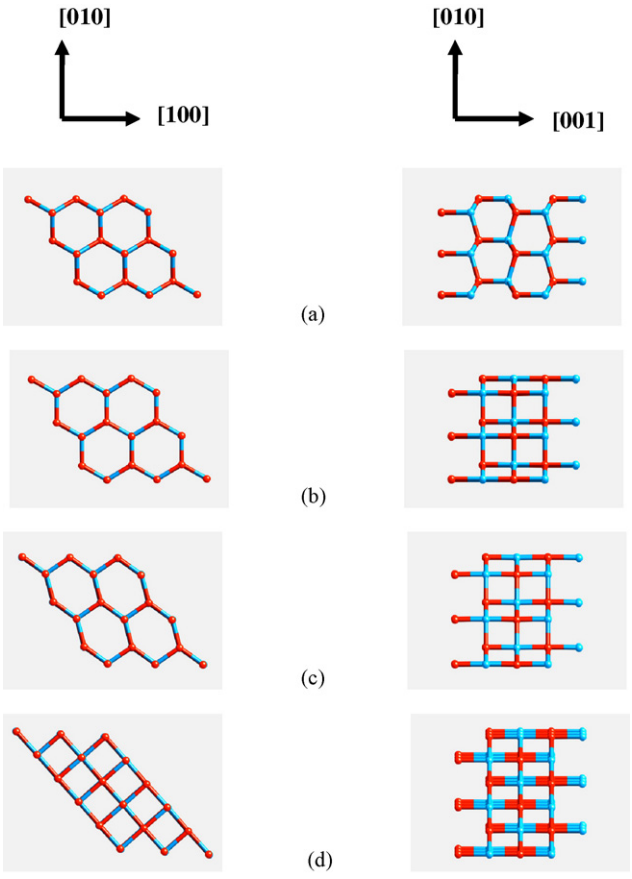

Fig. 2. At 120.0 GPa, evolution of the rocksalt structure at (a) zero MD step (wurzite phase) $\alpha = 120^\circ$, (b) 800 MD step (hexagonal phase) $\alpha = 120^\circ$, (c) 809 MD step (orthorhombic) $\alpha = 125^\circ$ and (d) 822 MD step (rocksalt structure) $\alpha = 135^\circ$.

In order to shed some light onto transformation mechanism at the atomistic level, we study the variations of the simulation cell vectors as a function of MD time step. Fig. 4 shows the modification of the simulation cell lengths and angles at 160.0 GPa. The simulation cell vectors **A**, **B**, and **C** are along the [1 0 0], [$\bar{1}$ 1 0] and [0 0 1] directions, respectively. The magnitude of these vectors is plotted in figure. As can be seen from figure, the transition proceeds in two steps. First the cell lengths decouple with one length decreasing (along [0 0 1] direction) with a corresponding increasing in the two lengths. This modification produces a fivefold coordinated hexagonal structure with the lattice parameters $a = b = 3.03$ Å, and $c = 3.79$ Å at the MD step 385 s, the system undergoes a shear deformation and the hexagonal angle α between **A** and **B** lattice vectors gradually changes from 120° about 135°. Consequently, |**B**| is increased while |**A**| is decreased. During this deformation, another intermediate state having *Cmcm* symmetry is determined when the hexagonal angle α reaches a value of about 125°. Its lattice constants are $a = 3.11$ Å, $b = 4.78$ Å, and $c = 3.77$ Å at the MD step 800. The lattice parameters and the atomic positions of the phases obtained at 120.0 GPa are summarized in Table 1. The evolution of the RS phase is illustrated in Fig. 2.

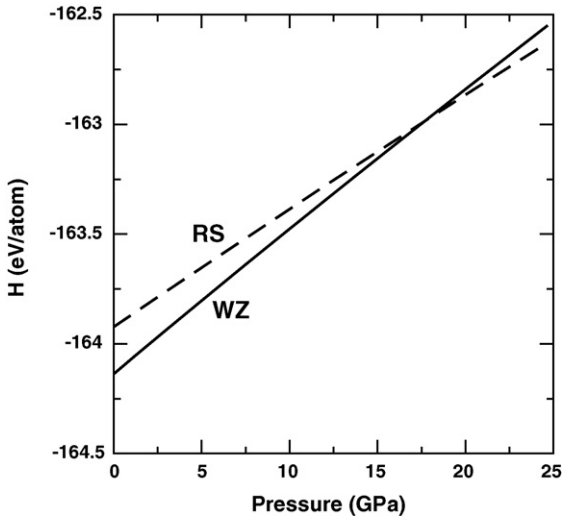

Fig. 3. Calculated enthalpy curve of the wurtzite and rocksalt structures as a function of pressure. The enthalpy curves crosses around 17.8 GPa, indicating a first-order phase transformation from wurtzite-to-rocksalt.

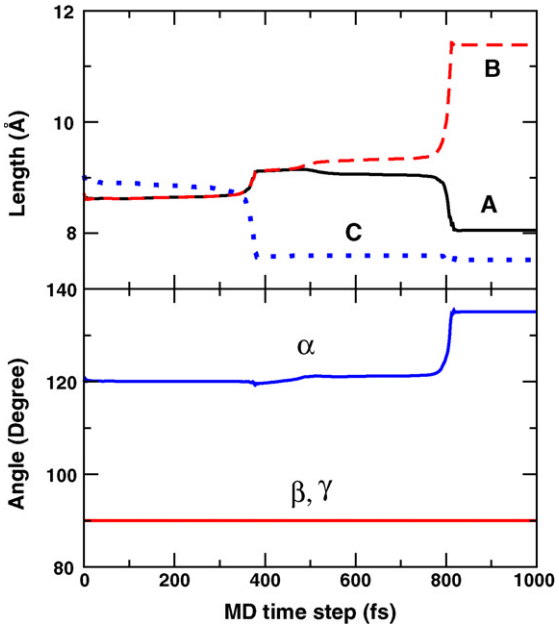

Fig. 4. Variation of the simulation cell lengths and angles as a function of MD time step. The simulation cell vectors **A**, **B**, and **C** are along the [1 0 0], [$\bar{1}$ 1 0] and [0 0 1] directions, respectively. The magnitude of these vectors is plotted in figure. Around 400 fs, the wurtzite structure is dramatically compressed along [0 0 1] direction while it is expanded along the other directions. Then system underwent shear deformation: the hexagonal angle α between **A** and **B** lattice vectors gradually changes from 120° about 135°. These deformations produce a rocksalt structure.

The mechanism observed in our simulation corresponds to "known hexagonal mechanisms." However, the *Cmcm* intermediate state has not been recognized for AlN before. Since the shear deformation is necessary to form the RS phase from the hexagonal state, the symmetry change is certainly anticipated during this distortion. Therefore, the WZ-to-RS phase change must be represented by at least two intermediate states (hexagonal and orthorhombic) for AlN.

Table 1
The atomic fractional coordinates and the lattice parameters of the phases formed at 120.0 GPa.

Structure	a (Å)	b (Å)	c (Å)	x	y	z
Hexagonal $P6_3/mmc$	3.03	3.03	3.79	Al: 0.3333 N: 0.3333	0.6667 0.6667	0.75 0.25
Orthorhombic *Cmcm*	3.31	4.78	3.77	Al: 0.0 N: 0.0	0.3174 0.6888	0.25 0.25
RS $Fm\bar{3}m$	3.78	3.78	3.78	Al: 0.5 N: 0.0	0.5 0.0	0.5 0.0

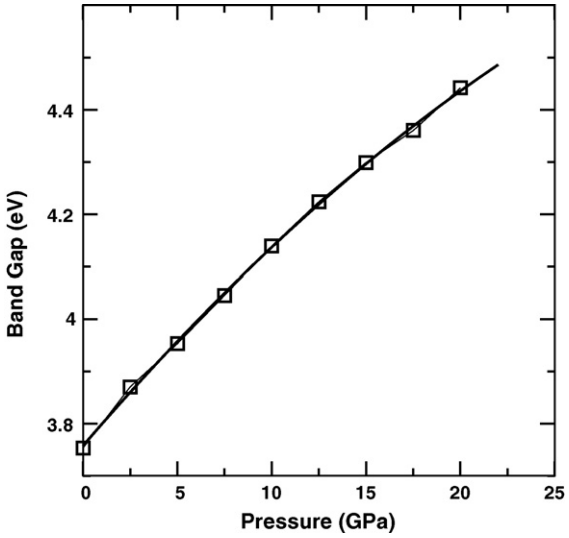

Fig. 5. The band gap energy as a function of applied pressure. The gap gradually increases with increasing pressure. The solid line corresponds to a least squares fit of a second-order polynomial.

We finally analyze the influence of the applied pressure on the electronic structure of AlN. We pressure AlN up to 20 GPa. For minimization of geometries, a variable-cell shape conjugate-gradient method under a constant pressure was used. For each value of the applied pressure, the lattice vectors and the atomic positions were optimized together until the stress tolerance was less than 0.5 GPa and the maximum atomic force was smaller than 0.01 eV Å^{-1}. The pressure–band gap relation between 0 GPa and 20 GPa is illustrated in Fig. 5 in which the solid line corresponds to a least squares fit of a second-order polynomial. At zero pressure, the GGA band gap as a difference between the top of the valence band and the bottom of the conduction band is about 3.75 eV. This value is comparable with the previous DFT calculations but as expected it is smaller than that of experimental result, 6.2 eV [5], mainly due to the well-known shortcoming of DFT within the GGA in describing excited states. The band gap obtained from the present calculation is therefore incomparable to the experimental result. However, despite the underestimation of the gap width, DFT often yields the variation of band gaps under pressure in good agreement with experiments. As seen from Fig. 5, the band gap energy increases progressively under pressure. With increasing pressure, the valence states near the band gap gradually shift to lower energies while the conduction states near the band gap gradually shift to higher energies, producing an increase in the band gap energy. The calculated linear and quadratic pressure coefficients are 41.9 meV/GPa and −0.4 meV/GPa, respectively. These values are close to 36.3 meV/GPa and −0.18 meV/GPa reported in the previous DFT calculations [12]. In order to calculate the deformation potential ($D = \Delta E_{gap}/\Delta V/V_0$ where $\Delta V = V - V_0$ and V_0 is the equilibrium volume at zero pressure), we plot the variation of the band gap as functional of volume in Fig. 6. The slope of the best fitting straight line gives an average deformation potential, −9.54 eV, for the WZ structured AlN, which is in very good agreement with the earlier DFT calculation results of −8.60 to −9.0 [10,35,36].

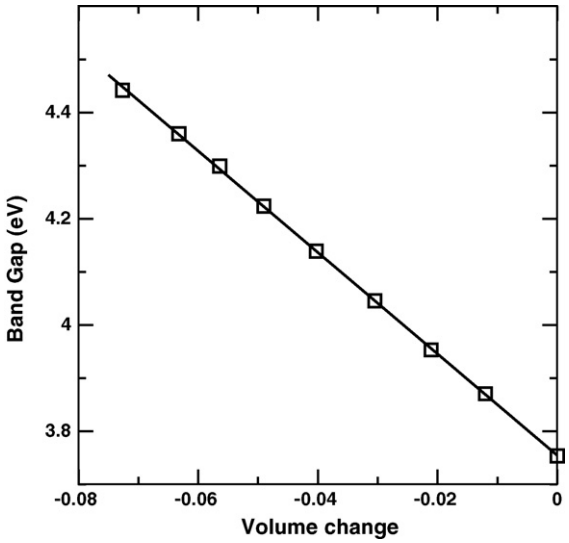

Fig. 6. Band gap energy as a function of volume change $\Delta V/V_0$, where $\Delta V = V - V_0$ and V_0 is the equilibrium volume at zero pressure. The solid line is the best linear fit.

4. Conclusions

We have carried out an *ab initio* constant pressure technique to study the pressure-induced phase transition in the WZ-structured AlN. A first-order phase change into a RS structure is successfully reproduced in the simulations. Furthermore, we establish an atomistic transformation mechanism and find that the transition proceeds in two steps. This transformation path is associated with two fivefold coordinated intermediates states within $P6_3/mmc$ and *Cmcm* symmetry. We also study the WZ-to-RS phase transition of AlN using the enthalpy calculations and find that our computed transition parameters and bulk properties are comparable with experimental and previous theoretical values. Additionally, we study the influence of the applied pressure on the electronic properties of AlN and find that the band gap energy gradually increases with increasing pressure. Our computed pressure coefficients and deformation potential are in good agreement with the earlier DFT calculations.

Acknowledgements

The simulations were performed during the visit of the author to Ahi Evran Üniversitesi, facilitated by the Scientific and Technical Research Council of Turkey (TÜBİTAK) BIDEB-2221. The calculations were run on Sacagawea, a 128 processor Beowulf cluster, at the University of Texas at El Paso.

References

[1] A.W. Weimer, G.A. Cochran, G.A. Eisman, J.P. Henley, B.D. Hook, L.K. Mills, T.A. Guiton, A.K. Knudsen, N.R. Nicholas, J.E. Volmering, W.G. Moor, J. Am. Ceram. Soc. 77 (1994) 3.
[2] A.V. Virkar, T.B. Jackson, R.A. Cutler, J. Am. Ceram. Soc. 72 (1989) 2031.
[3] T.J. Mroz Jr., Ceram. Bull. 71 (1992) 782.
[4] J.H. Edgar (Ed.), Properties of Group-III Nitrides, IEE, London, 1994, EMIS Datareviews Series.
[5] Lev I. Berger, Semiconductor Materials, CRC Press, New York, 1997, p. 124.
[6] Q. Xia, H. Xia, A.L. Ruoff, J. Appl. Phys. 73 (1993) 8193.
[7] L. Hultman, S. Benhenda, G. Radnoczi, J.-E. Sundgren, J.E. Greene, I. Petrov, Thin Solid Films 215 (1992) 152.
[8] M. Ueno, A. Onodera, O. Shimomura, K. Takemura, Phys. Rev. B 45 (1992) 10123.
[9] S. Uehara, T. Masamoto, A. Onodera, M. Ueno, O. Shimomura, K. Takemura, J. Phys. Chem. Solids 58 (1997) 2093.
[10] N.E. Christensen, I. Gorczyca, Phys. Rev. B 47 (1993) 4307.
[11] J. Serrano, A. Rubio, E. Hernandez, A. Munoz, A. Mujica, Phys. Rev. B 62 (2000) 16612.
[12] P.E. Van Camp, V.E. Van Doren, J.T. Devreese, Phys. Rev. B 44 (1991) 9056.
[13] A.M. Saitta, F. Decremps, Phys. Rev. B 70 (2004) 035214.
[14] C.C. Silva, H.W. Leite Alves, L.M.R. Scolfaro, J.R. Leite, Phys. Stat. Sol. C 2 (2005) 2468.
[15] I. Gorczyca, N.E. Christensen, P. Perlin, I. Grzegory, J. Jun, M. Bockowski, Solid State Commun. 79 (1991) 1033.
[16] J. Cai, N. Chen, Phys. Rev. B 75 (2007) 134109.
[17] H.Y. Xiao, F. Gao, L.M. Wang, X.T. Zu, Y. Zhang, W.J. Weber, Appl. Phys. Lett. 92 (2008) 241909.

[18] H. Liu, Y. Ding, M. Somayazulu, J. Qian, J. Shu, D. Häusermann, H.K. Mao, Phys. Rev. B 71 (2005) 212103.
[19] F. Shimojo, S. Kodiyalam, I. Ebbsjö, R.K. Kalia, A. Nakano, P. Vashishta, Phys. Rev. B 70 (2004) 184111.
[20] M.D. Knudson, Y.M. Gupta, A.B. Kunz, Phys. Rev. B 59 (1999) 11704.
[21] M. Grünward, E. Rabani, C. Dellago, Phys. Rev. Lett. 96 (2006) 255701.
[22] S.H. Tolbert, A.P. Alivisatos, J. Chem. Phys. 102 (1995) 4642.
[23] M. Durandurdu, Phys. Rev. B 75 (2007) 235204.
[24] J.P. Perdew, K. Burke, M. Ernzerhof, Phys. Rev. Lett. 77 (1996) 3865.
[25] P. Ordejòn, E. Artacho, J.M. Soler, Phys. Rev. B 53 (1996) 10441.
[26] N. Troullier, J.M. Martins, Phys. Rev. B 43 (1991) 1993.
[27] M. Parrinello, A. Rahman, Phys. Rev. Lett 45 (1980) 1196.
[28] R. Hundt, J.C. Schön, A. Hannemann, M. Jansen, J. Appl. Crystallogr. 32 (1999) 413.
[29] H. Shultz, K.H. Thiemann, Solid State Commun. 23 (1977) 815.
[30] S. Strite, H. Morkoc, J. Vac. Sci. Technol. B 10 (1992) 1237.
[31] K. Karch, F. Bechstedt, Phys. Rev. B 56 (1997) 7404.
[32] A. Hung, S.P. Russo, D.G. McCulloch, S. Prawer, J. Chem. Phys. 120 (2004) 4890.
[33] M.G.M. Armenta, R.S. Armando, M.A. Borja, Phys. Rev. B 62 (2000) 4890.
[34] R. Martoñák, A. Laio, M. Parrinello, Phys. Rev. Lett. 90 (2003) 75503.
[35] J.-M. Wagner, F. Bechstedt, Phys. Rev. B 66 (2002) 115202.
[36] K. Kim, W.R.L. Lambrecht, B. Segall, Phys. Rev. B 53 (16) (1996) 310.